Taylor & Francis
Taylor & Francis Group

ORIGINAL RESEARCH

🔓 OPEN ACCESS  Ⓜ Check for updates

# *In vivo* dynamics and anti-tumor effects of EpCAM-directed CAR T-cells against brain metastases from lung cancer

Tao Xu[a]*, Philipp Karschnia[b,c]*, Bruno Loureiro Cadilha[d]*, Sertac Dede[a], Michael Lorenz[e], Niklas Seewaldt[b], Elene Nikolaishvili[b], Katharina Müller[a], Jens Blobner[b,c], Nico Teske[b,c], Julika J. Herold[b], Kai Rejeski[c,f], Sigrid Langer[a], Hannah Obeck[d], Theo Lorenzini[d], Matthias Mulazzani[g], Wenlong Zhang[a], Hellen Ishikawa-Ankerhold[e], Veit R. Buchholz[h], Marion Subklewe[f], Niklas Thon[b,c], Andreas Straube[a], Joerg-Christian Tonn[b,c], Sebastian Kobold[d§], and Louisa von Baumgarten[a,b,c§]

[a]Department of Neurology, University Hospital of the Ludwig-Maximilians-University Munich, Munich, Germany; [b]Department of Neurosurgery, University Hospital of the Ludwig-Maximilians-University Munich, Munich, Germany; [c]German Cancer Consortium (DKTK), Partner Site Munich, Munich, Germany; [d]Department of Medicine IV, Division of Clinical Pharmacology and Center of Integrated Protein Science Munich, University Hospital of the Ludwig-Maximilians-University Munich, Munich, Germany; [e]Department of Medicine I, University Hospital of the Ludwig-Maximilians-University Munich, Munich, Germany; [f]Department of Medicine III, University Hospital of the Ludwig-Maximilians-University Munich, Munich, Germany; [g]Immunology Division, Walter and Eliza Hall Institute of Medical Research, Parkville, Australia; [h]Institute for Medical Microbiology, Immunology and Hygiene, Technische Universitaet Muenchen (TUM), Munich, Germany

## ABSTRACT

Lung cancer patients are at risk for brain metastases and often succumb to their intracranial disease. Chimeric Antigen Receptor (CAR) T-cells emerged as a powerful cell-based immunotherapy for hematological malignancies; however, it remains unclear whether CAR T-cells represent a viable therapy for brain metastases. Here, we established a syngeneic orthotopic cerebral metastasis model in mice by combining a chronic cranial window with repetitive intracerebral two-photon laser scanning-microscopy. This approach enabled *in vivo*-characterization of fluorescent CAR T-cells and tumor cells on a single-cell level over weeks. Intraparenchymal injection of Lewis lung carcinoma cells (expressing the tumor cell-antigen EpCAM) was performed, and EpCAM-directed CAR T-cells were injected either intravenously or into the adjacent brain parenchyma. In mice receiving EpCAM-directed CAR T-cells intravenously, we neither observed substantial CAR T-cell accumulation within the tumor nor relevant anti-tumor effects. Local CAR T-cell injection, however, resulted in intratumoral CAR T-cell accumulation compared to controls treated with T-cells lacking a CAR. This finding was accompanied by reduced tumorous growth as determined per *in vivo*-microscopy and immunofluorescence of excised brains and also translated into prolonged survival. However, the intratumoral number of EpCAM-directed CAR T-cells decreased during the observation period, pointing toward insufficient persistence. No CNS-specific or systemic toxicities of EpCAM-directed CAR T-cells were observed in our fully immunocompetent model. Collectively, our findings indicate that locally (but not intravenously) injected CAR T-cells may safely induce relevant anti-tumor effects in brain metastases from lung cancer. Strategies improving the intratumoral CAR T-cell persistence may further boost the therapeutic success.

## Background

Brain metastases arise from hematogenous dissemination of malignant cells from an extracranial neoplasm to the cerebral vasculature. Patients with lung cancer are at a particularly high risk, and 30–50% of affected individuals are expected to develop brain metastases during the course of their disease.[1],[2] This number might even increase in the next decades given that therapeutic advances for lung cancer involving immunotherapeutic or targeted agents have resulted in prolonged disease courses.[3] Although control of extracranial disease can often be achieved using such agents, a considerable number of patients succumb to their intracranial tumor.[4] Novel therapeutic strategies for the treatment of lung cancer brain metastases are therefore urgently warranted.

Chimeric Antigen Receptor (CAR) T-cells represent a powerful class of cell-based immunotherapy for advanced malignancies. CAR incorporates antigen-recognition moieties and co-stimulatory domains, which re-direct killing activity of an autologous T-cell population against a specific tumor cell antigen following genetical modification. Particularly, the B-cell antigen CD19 has proven as an effective target in patients with hematological neoplasms,[5] and several CAR T-cell products have been approved in the United States and Europe. Substantial efforts to translate such therapy into treatment for solid tumors including primary as well as secondary

brain tumors have been made,[6,7] and numerous potential targets such as the epithelial cell adhesion molecule (EpCAM) presented on the surface of lung cancer cells have been discussed in this context.[8] EpCAM is overexpressed in about 50% of non-small cell lung cancer.[9] Its overexpression is typically also conserved in metastatic disease[10] and in some cancers even upregulated in metastases compared to primary tumors.[11] Although theoretically promising, it remains unclear whether (EpCAM-directed) CAR T-cells may indeed constitute an effective therapeutic avenue for brain metastases from lung cancer.

In this study, we combined intracerebral two-photon laser scanning microscopy and a chronic cranial window model to establish a syngeneic orthotopic brain metastasis model. This fully immunocompetent murine model allowed repetitive visualization of fluorescent CAR T-cells and cancer cells at single-cell resolution. Based on this approach, we were able to analyze the *in vivo* dynamics, persistence, and anti-tumor effects of systemically and intraparenchymally injected EpCAM-directed CAR T-cells against established brain metastases from lung cancer.

## Methods

### Animals

Male C57BL/6 mice (Charles River Laboratories) at the age of 8–14 weeks were used for tumor implantation experiments and isolation of T-cells. After surgical procedure, the animals were housed one per cage and had access to tap water and standard pellet food *ad libitum*. All animal experiments were approved by the local governmental animal care committee (Regierung von Oberbayern; permission number: 02–20-44) and conducted in accordance with European legislation on protection of animals and NIH Guidelines (NIH Publication #85-23 Rev. 1985).

### Cell lines

The murine Lewis Lung carcinoma cell line LL/2 was purchased from the European Collection of Authenticated Cell Cultures (ECACC; catalog number: #90-0201-04). Cells were cultured in DMEM (#41-965-039, Thermo Fisher) supplemented with 2 mM glutamine and 10% FCS (#S0615, Biochrom). Testing for mycoplasma infection was regularly performed. To keep genetic drift at minimum, cells were maintained in culture for up to 4 weeks after thawing.

### Tumor cell line generation

A PCR product containing the sequence of tdTomato (vector ptdTomato; #63-2531, TaKaRa Clontech) was cloned into the lentiviral expression vector pLVX-IRES-neo (LentiX-Bicistronic Expression System; #63-2181, TaKaRa Clontech) to generate a pLVX-tdTomato-IRES-Neo construct. Notably, a resistance-sequence for G418-sulfate is contained in the lentiviral expression vector. The resulting nucleotide pLVX-tdTomato-IRES-Neo was verified by

Sanger sequencing and restriction enzyme digestion.[12] LL/2 was transfected with pLVX-tdTomato-IRES-Neo using lipofection (Lipofectamine 3000; Thermo Fisher Scientific). $^{tdt}$LL/2 was enriched by cultivation in selection medium containing G418-sulfate (#A2912; Biochrom) and by repetitive FACS sorting. As previously described in detail,[13] $^{tdt}$LL/2 cells were stably transduced with a pMXs vector containing the full-length murine EpCAM (UNIPROT entry: #Q99JW5) cDNA to generate the EpCAM-overexpressing cell line $^{EpCAM/tdt}$LL/2.

### Retroviral transduction vectors

The anti-EpCAM-CAR construct was previously described by Lesch & Blumenberg *et al.*[14] and Cadilha *et al.*[15], and consists of a single-chain variable fragment that recognizes the murine EpCAM antigen (clone G8.8), fused to the transmembrane and signaling domains of murine CD28 and murine wildtype CD3zeta (with three intact immunoreceptor tyrosine-based activation motifs) in a pMP71 backbone. The anti-EpCAM-CAR-GFP construct consists of anti-EpCAM-CAR fused to GFP via a self-cleaving 2A sequence. GFP-expressing, EPCAM-directed CAR T-cells ($^{EpCAM/GFP}$CAR T-cells) were generated; and T-cells transduced by a vector containing GFP only were used as controls ($^{GFP}$T-cells).

### Isolation and transduction of T-cells

T-cells were isolated from spleens of C57BL/6 mice and were enriched with a mouse CD8a+ T-cell isolation kit (#130-104-075, Miltenyi Biotec). Transduction of primary murine T-cells was conducted as previously described.[14–16] In short, supernatants containing the virus of interest were used for transduction on two consecutive days (**Supplementary Figure 1A-C**). During virus generation, primary murine T-cells were activated with anti-CD28 (#16-0281-86, Thermo Fisher) and anti-CD3 antibodies (#16-0031-86, Thermo Fisher) in murine T-cell medium supplemented with IL-2 (#20-002, Peprotech) and β-mercaptoethanol (#21-9850-23, Gibco) for 24 hours. During the transduction process, T-cells were stimulated with Dynabeads Mouse T-Activator CD3/CD28 (#11-452D, Thermo Fisher). Transduced murine T-cells were expanded with murine T-cell medium and supplemented with IL-2 and β-mercaptoethanol, and maintained at a concentration of $1 \times 10^6$ cells per mL every second day. *Ex vivo* culture of T-cells was 4–7 days. Following retroviral transduction and expansion, $^{EpCAM/GFP}$CAR T-cells were selected by GFP-positivity utilizing a MolFloll Cell Sorter (Beckman Coulter) after exclusion of dead cells.

### IFN-γ release cytotoxicity assay

To confirm proper function of CAR T-cells, $2 \times 10^4$ $^{EpCAM/tdt}$LL/2 was co-cultured with $2 \times 10^5$ $^{EpCAM/GFP}$CAR T-cells in 200 μL culture medium (RPMI1640 supplemented with 10% FCS, 1%P/S, 1% Sodium Pyruvate and 0,1% HEPES). After 24-48 hours, levels of IFN-γ in the supernatant were analyzed using an ELISA assay (#55-5138, BD Biosciences).

## Cranial window preparation

As previously described in detail,[17,18] chronic cranial windows were prepared in male C57BL/6 mice. Briefly, a circular part of the calvarium (diameter: 5.5 mm) was removed and the dura was gently separated from the leptomeninges to achieve optimal image resolution. The cortical surface was covered with saline, and a sterile round cover glass (diameter: 6 mm) was attached to the cranium. To facilitate optimal head positioning during imaging, a custom-made plastic ring (diameter: 8 mm) was also glued to the skull. Buprenorphine (0.1 mg/kg; every 8 hours) was injected for two postoperative days to ensure analgesia. Prior to further experiments, a postoperative recovery time of 28 days was granted to prevent postoperative inflammation or alterations of the microcirculation.

## Intraparenchymal injection of tumor cells and CAR T-cells

To simulate cerebral growth of brain metastases, $2.5 \times 10^3$ EpCAM/tdtLL/2 was resuspended in 1 μL PBS and stereotactically injected into the left hemisphere at predefined coordinates (1 mm lateral to the sagittal sinus and 2 mm posterior to the bregma; intraparenchymal depth: 1.5 mm). For intravenous injection, $2.0 \times 10^6$ EpCAM/GFPCAR T-cells concentrated in 0.2 mL PBS were injected into the tail vein 7 days after tumor cell injection. For intracerebral injection, $2.0 \times 10^5$ $^{EpCAM/GFP}$CAR T-cells concentrated in 1–2 μL PBS were injected 1 mm posterior to the tumor cell injection point (intraparenchymal depth: 1 mm) (Figure 1a) 7 days after tumor cell injection. Intracerebral injections of tumor cells and CAR T-cells were either done after careful removal of the cover glass (for mice allocated to *in vivo* imaging and subsequent immunofluorescence analyses) or through a burr hole (for mice allocated to survival experiments).

## In vivo two-photon laser scanning microscopy and image acquisition

Metastatic growth was followed by repetitive *in vivo* microscopy whenever quality of the chronic cranial window allowed. For this purpose, a TrimScope multiphoton microscopy platform (LaVision Biotech TrimScope I) equipped with a MaiTai-laser (wavelength 690–1040 nm; Spectra Physics, Newport) and a 4-times objective (numerical aperture: 0.28; XLFluor, Olympus) or a 20-times water immersion objective (numerical aperture: 0.95; XLUMPlanFl, Olympus) was used. Mice were placed on a heating mat during imaging sessions, anesthesia was established with 1% to 2% isoflurane in oxygen adjusted to the breathing rate, and the cranial plastic ring was tightly secured in a custom-made holding device to ensure minimal movements due to breathing. Prior to *in vivo* microscopy, 100 μL fluorescein isothiocyanate (FITC)-dextran (10 mg/mL, 2 MDa molecular mass; Sigma-Aldrich) was injected into the tail vein for intravascular plasma staining and, thus, visualization of cerebral blood vessels when appropriate. Recordings were made every 5 μm at a wavelength of 920 nm, and image resolution was set at $1024 \times 1024$ pixels. For statistical analyses, 3D image stacks with x/y/z-dimensions of $450 \times 450 \times 400$ μm were acquired and imaging started at the cortical surface (as defined by detection of the arachnoid fibers using second harmonic imaging). For dynamic analyses, 3D image stacks with x/y/z-dimensions of $450 \times 450 \times 66$ μm were repetitively acquired over 30 minutes (one recording every 30 seconds) and imaging started 100 μm below the cortical surface.

## Image analysis

Imaris v8.2 (Bitplane AG) and ImageJ/Fiji (NIH) were used for image analysis. Raters were blinded to group allocation until final data analyses were done. CAR T-cells were detected *in vivo* using their green fluorescent signal, and tumor cells
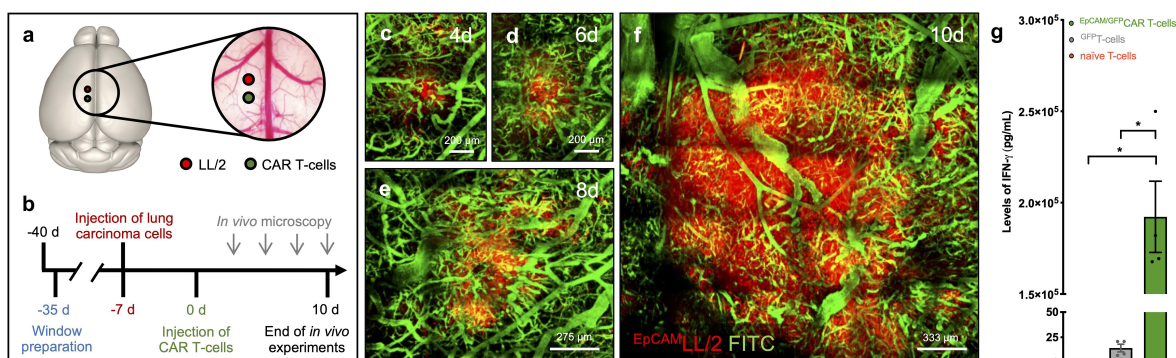


**Figure 1. Experimental protocol and *in vivo* model of brain metastases from lung cancer.** A: Position of the chronic cranial window (circle; diameter: 5.5 mm) and the injection sites of the tumor cells (red) as well as the locally injected (CAR) T-cells (green). For intravenous experiments, (CAR) T-cells were injected into the tail vein. The 3dBAR plugin of the Scalable Brain Atlas (Bakker *et al.* in Neuroinformatics, 2015)[19] was used to create the panel, and the panel has been adapted from Zhang & Karschnia & von Mücke-Heim *et al.* (in Neoplasia, 2021).[12] B: Schematic representation of the experimental design. C-F: Intracerebral growth of $^{EpCAM/tdt}$LL/2 (red) following intraparenchymal tumor cell injection. Images represent mosaics of multiple maximum intensity projections with 400 μm depth from the brain surface. Blood vessels are highlighted via intravascular plasma staining using FITC-dextran (green). Note that the day count refers to the day after CAR T-cell injection (which is seven days after tumor injection). Scale bars: C, D: 200 μm; E: 275 μm; F: 333 μm. G: ELISA performed for murine IFN-γ on supernatants after co-culture of $^{EpCAM/tdt}$LL/2 with naïve T-cells (orange), $^{GFP}$T-cells (gray), or $^{EpCAM/GFP}$CAR T-cells (green) for 24 hours (n = 4). Mean ± SEM. *$p \leq .05$.

were identified using their red fluorescent signal. For calculation of tumor size *in vivo*, the 2D tumor area was delineated during epifluorescence microscopy. In case of multiple tumors, individual tumor areas were added. For calculation of CAR T-cell density and dynamics, the number and velocity of CAR T-cells were determined from the 3D image stacks obtained during *in vivo* two-photon laser scanning microscopy.

### Immunofluorescence analyses

Excised brains were stored in PFA 4%, and the water was subsequently removed from the samples by incubation in ascending sucrose series until equilibration was reached. Samples were then transferred to the gas phase of liquid nitrogen for 5 minutes and eventually into −80°C. Finally, brains were cut into 15 μm-thick sections spaced 495 μm apart.

For analyses on (CAR) T-cells and tumor growth, sections were only stained with a polyclonal rabbit-anti-DS-red antibody (#632496; 1:200, Clontech) to highlight the tdTomato-signal of tumor cells and with a chicken-anti-GFP-antibody (#AB13970; 1:200, Abcam) to detect the GFP-signal of the CAR T-cells. As secondary antibody, a donkey-anti-rabbit AlexaFluor®−594 antibody (#A21207; 1:100, Invitrogen) and a goat-anti-chicken AlexaFluor®−488 antibody (#AB150169; 1:200, Abcam) were used. For analyses on the immunosuppressive tumor microenvironment or expression of EpCAM, sections were additionally stained with either a rabbit-anti-Iba1 antibody (#01919741; 1:500, Wako), a rat-anti-EpCAM antibody (#145791; 1:400, eBioscience) or goat-anti-CD206 antibody (#AF2535; 1:4000, R&D), while the endogenously expressed TdTomato- and GFP-signal was not further enhanced. Chicken-anti-rabbit AlexaFluor®−647 antibody (#A21443; 1:100, Invitrogen), chicken-anti-rat AlexaFluor®−647 antibody (#A21472; 1:100, Invitrogen), or donkey-anti-goat AlexaFluor®−647 antibody (#A21447; 1:200, Invitrogen) were applied as secondary antibodies, respectively. The sections were placed in a humidified incubation box and incubated overnight at 4°C with the primary antibody. The labeling with the secondary antibody was performed at room temperature for 1 hour. Cell nuclei were stained with DAPI (#236276; 1:1000, Roche).

Sections were assessed using a Zeiss AxioImager.M2 upright-microscope (Carl Zeiss Microscopy). To quantify the tumor volume and CAR T-cell density per immunofluorescence, we manually delineated the tumor based upon the fluorescence signal using Zen Lite software package (version 2.3; Carl Zeiss Microscopy). Total tumor area per slice was multiplied with a thickness of 495 μm, and addition of all values yielded the total tumor volume. CAR T-cell density was determined in total cells per total tumor volume, and intratumoral CAR T-cells were further specified as being present either in the tumor core or in the border zone of the tumor (defined as the tumor area with a distance of 0–10 μm from the outer tumor border). One to two random tumor slices per mouse were selected for analyses on CD206 and Iba1, and density of CD206- and Iba1-positive cells was calculated per tumor area. Again, positive cells were assigned as being present either in the tumor core or in the border zone of the tumor. Tumoral EpCAM expression was semi-quantitatively determined for two randomly selected tumor slices per mouse using the following scoring system: 0–25, 26–50, 51–75, or 76–100% EpCAM-positive tumor cells (tumor cells were identified by detection of their inherent tdTomato-signal).

### Experimental protocol

For *in vivo* microscopy, tumor cells were injected into the brain parenchyma through the cranial window. For analysis on intravenous injection of CAR T-cells, mice were randomly allocated to receive either $^{EpCAM/GFP}$CAR T-cells (n = 6) or $^{GFP}$T-cells as controls (n = 6) 7 days after tumor implantation. For analysis on intracerebral injection of CAR T-cells, mice randomly either received $^{EpCAM/GFP}$CAR T-cells (n = 10) or $^{GFP}$T-cells as controls (n = 8) 7 days after tumor implantation. Two-photon laser scanning microscopy was performed on days 4, 6, 8, and 10 after CAR T-cell injection (and additional imaging on day −1 for baseline tumor area measurement by epifluorescence) (Figure 1b). Blood sampling of the facial vein was performed on days 4 and 10 after CAR T-cell injection. Blood was collected in ethylenediaminetetraacetic acid-coated capillary tubes and assessed for the presence of intravascular CAR T-cells using FACS analysis. Animals were sacrificed at the end of *in vivo* microscopy experiments on day 10 (to allow comparison between tumor size per immunofluorescence; or when termination criteria including neurologic symptoms attributed to tumor growth were met) by intracardiac injection of 0.9 % NaCl solution followed by PFA 4%, and brains were excised for further immunofluorescence analyses. For survival experiments in intracerebrally injected CAR T-cells, tumor cell and CAR T-cell injection ($^{EpCAM/GFP}$CAR T-cells: n = 8; $^{GFP}$T-cells: n = 9) was performed through a burr hole. Mice were followed until termination criteria were met.

### Statistics

Statistical analysis was performed using GraphPad Prism software (v9.0). Normal distribution and equal variance of data were tested using the D'Agostino-Pearson omnibus normality-test. Differences were assessed the Student's t-test (parametric data) or by the Mann–Whitney U-test (non-parametric data). If not indicated otherwise, all values are expressed as mean ± standard error of the mean (SEM). Categorical variables are described in absolute numbers and percentages. Relationships between categorical variables were analyzed using the $\chi^2$-test. Survival was calculated using Kaplan–Meier survival analysis and log-rank test. The significance level was set at $p \leq 0.05$. All data needed to evaluate the conclusions of the current study are present in the main manuscript.

## Results

### Development of a murine model for in vivo-imaging of CAR T-cells in brain metastases from lung cancer

Implantation of a chronic cranial window was well tolerated, and window quality reliably allowed for repetitive *in vivo* imaging using two-photon laser scanning microscopy. After $^{EpCAM/tdt}$LL/2 was intracranially injected into the brain parenchyma, tumor cells were detected based upon their red

fluorescence signal. All mice had visible tumor take 6 days after the tumor cell injection; and rapid growth of solitary lesions was seen in the following days (Figure 1c-f). Fluorescence intensity remained high until the end of the in vivo experiments. We generated GFP-expressing [EpCAM/GFP]CAR T-cells recognizing EpCAM which is presented on the surface of the [EpCAM/tdt]LL/2 tumor cell line. Mean transduction efficiency for [EpCAM/GFP]CAR T-cells measured by flow cytometry was 58%, and EpCAM-specific cytotoxicity of the CAR T-cells was confirmed in vitro by co-culturing with EpCAM-expressing [EpCAM/tdt]LL/2 target cells (Figure 1g). Whereas undirected T-cells did not exert relevant killing activity, the co-culture with [EpCAM/GFP]CAR T-cells resulted in substantial tumor cell lysis translating into increased levels of released IFN-γ. Notably, the in vitro anti-tumor effects of [EpCAM/GFP]CAR T-cells were dependent on the exact "effector cell:tumor cell"-ratio (**Supplementary Figure 1D-F**). [EpCAM/GFP]CAR T-cells were visualized in vivo using their green fluorescence signal, and no neurotoxic or systemic side effects after (systemic or local) [EpCAM/GFP]CAR T-cell injection were observed.

### In vivo dynamics and anti-tumor effects of CAR T-cells after systemic injection

Exponential tumor growth was seen in mice that received [GFP]T-cells which served as controls but also in mice that received intravenously injected [EpCAM/GFP]CAR T-cells (Figure 2a, b). However, intratumoral [EpCAM/GFP]CAR T-cells were detected in higher densities than control [GFP]T-cells as early as 4 days after intravenous injection (Figure 2c, d); no differences in density were detected between the two groups at lateral stages (Figure 2e). Overall, the intratumoral EpCAM/GFPCAR T-cell density was markedly lower than after intracranial injection. Accordingly, we did not find any evidence of beneficial anti-tumor effects of intravenously injected [EpCAM/GFP]CAR T-cells against the rapid brain tumor growth through the entire observation period (figure 2f). In blood samples taken on days 4 and 10 after intravenous (CAR) T-cell injection, we did not find evidence of intravascular expansion of [EpCAM/GFP]CAR T-cells and [EpCAM/GFP]CAR T-cell numbers were lower than [GFP]T-cells numbers which might be interpreted as sign of insufficient [EpCAM/GFP]CAR T-cell proliferation or extravasation (**Supplementary Figure 1 G**), although the final mechanisms remain elusive.

### In vivo dynamics of CAR T-cells after intraparenchymal injection

After injection of CAR T-cells into the cerebral parenchyma adjacent to the tumor, the cells migrated in large numbers toward the brain tumor within days (Figure 3a-d). As a sign of successful tumor infiltration, intratumoral density of [EpCAM/GFP]CAR T-cells on day 4 after CAR T-cell injection exceeded the number of [GFP]T-cells (Figure 3e). Although a considerable number of [EPCAM/GFP]CAR T cells was also found in the healthy contralateral hemisphere, no significant differences were found compared to controls (figure 3f). This might indicate that the increased intratumoral [EPCAM/GFP]CAR T-cell numbers are a result of enhanced proliferation or migration rather than by

passive diffusion of CAR T-cells from the injection site alone. Notably, both intratumoral and contralateral densities were highest as early as 4 days after [EpCAM/GFP]CAR T-cell injection; and the numbers successively decreased during the observation period. T-cell receptor (TCR)-mediated anti-tumor cytotoxicity can be characterized by long-lasting contacts between effector immune and tumor cells.[20,21] Accordingly, we found lower T-cell velocities in mice receiving [EpCAM/GFP]CAR T-cells (Figure 3g, h). In addition, we assessed blood samples taken on days 4 and 10 after intracranial CAR T-cell injection for the presence of CAR T-cells. We were not able to detect any intravascular [EpCAM/GFP]CAR T-cells (or [GFP]T-cells in controls) (**Supplementary Figure 1 H**) and therefore did not find evidence of significant CAR T-cell extravasation from the brain parenchyma into the systemic vasculature.

### Effects of intraparenchymal CAR T-cell injection on tumor growth and survival

At the time of CAR T-cell injection, there were no differences between the groups regarding 2-dimensional tumor area determined during in vivo microscopy using epifluorescence (Figure 4a-b). Whereas control mice treated with [GFP]T-cells showed exponential and rapid tumor growth during the observation period, treatment with [EpCAM/GFP]CAR T-cells resulted in decreased growth accompanied by an accumulation of intratumoral [EpCAM/GFP]CAR T-cells (Figure 4c-k). In four out of ten mice (40%) treated with [EpCAM/GFP]CAR T-cells, we could not detect tumors through in vivo microscopy at the end of the experiment. The absence of a tumor was further confirmed per post-mortem histology in three of those four mice. Moreover, only one animal (10%) receiving [EpCAM/GFP]CAR T-cells developed a tumor with $\geq 5$ mm$^2$ tumor area, while seven out of eight control mice (87.5%) were found to have large tumors with a 2-dimensional area of $\geq 5$ mm$^2$. In line with these findings, in a separate set of experiments we could demonstrate a longer median survival in mice receiving [EpCAM/GFP]CAR T-cells compared to mice receiving [GFP]T-cells (Figure 4l). Interestingly, we also encountered long-term (disease-free) survival in a mouse for up to the maximal observation limit of 83 days (imposed by animal care regulations) after [EpCAM/GFP]CAR T-cell injection.

### CAR T-cell effects and intratumoral distribution below visualizable depths in mice which received intraparenchymal CAR T-cell injections

Two-photon laser scanning microscopy allowed in vivo observation of CAR T-cell dynamics up to a parenchymal depth of 400 μm. Immunofluorescence analyses of excised brains enabled further analysis of the anti-tumor effects and spatiotemporal distribution of locally injected CAR T-cells in the entire brain. At the end of the in vivo microscopy, nine brains of mice receiving locally injected [EpCAM/GFP]CAR T-cells and eight brains of mice receiving locally injected [GFP]T-cells could be evaluated using immunofluorescence. Tumors were found in six mice treated with locally injected [EpCAM/GFP]CAR T-cells (67%) and in all control mice based upon the detection of the inherent fluorescent signal of tumor cells. Tumor volumes determined via immunofluorescence were lower among mice
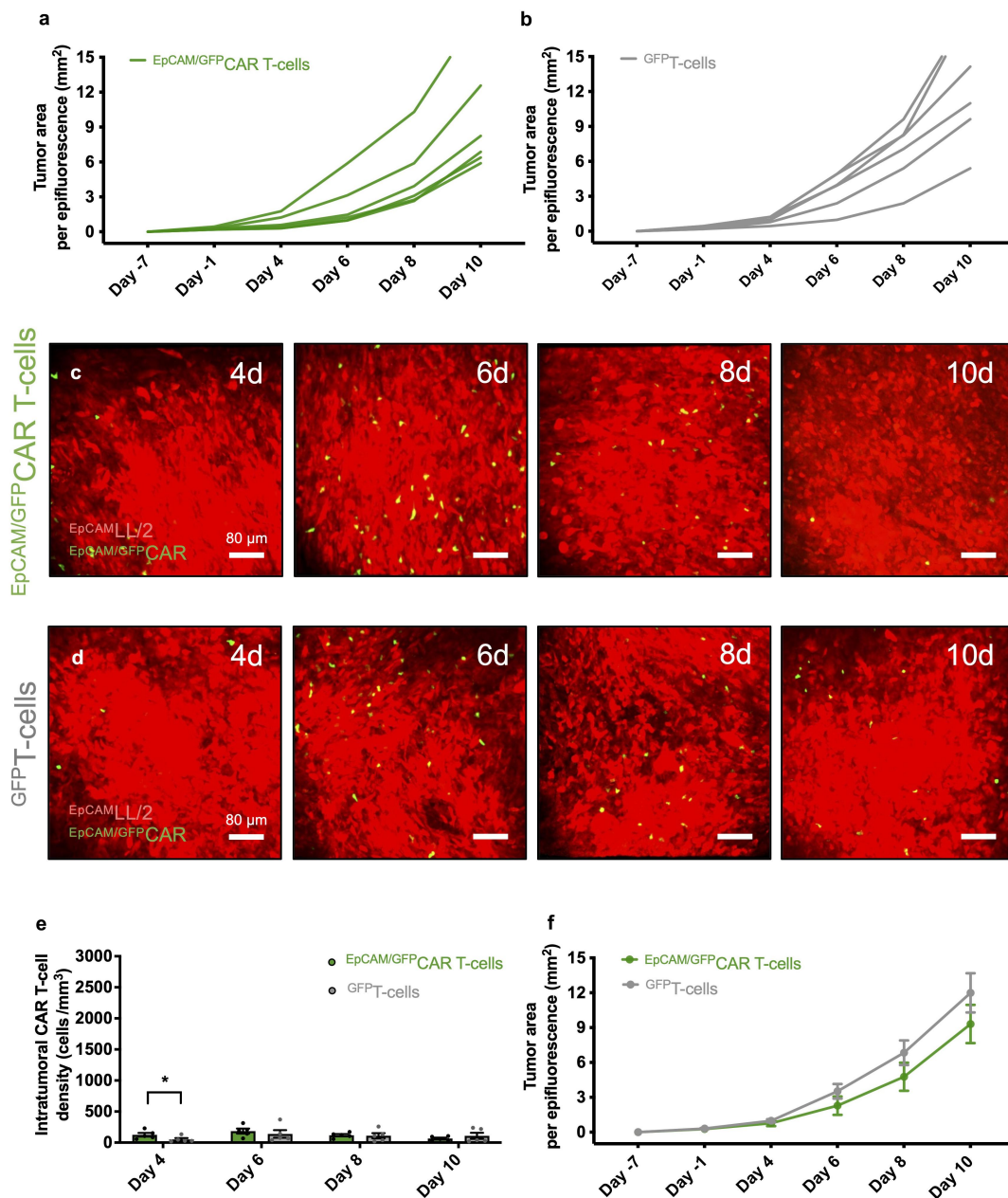
**Figure 2. CAR T-cell density and anti-tumor effects after intravenous CAR T-cell injection.** A, B: Individual tumor areas (mm$^2$) measured by *in vivo* microscopy using epifluorescence on days −1, 4, 6, 8, and 10 after intravenous injection of $^{EpCAM/GFP}$CAR T-cells (A; n = 6) or $^{GFP}$T-cells (B; n = 6). C, D: Representative *in vivo* images of brain tumors (red) on days 4, 6, 8, and 10 after intravenous injection of $^{EpCAM/GFP}$CAR T-cells (green; C) or $^{GFP}$T-cells (green D) using two-photon laser scanning microscopy (maximum intensity projections with 400 μm depth from the brain surface). Note the slightly increased $^{EpCAM/GFP}$CAR T-cell numbers on day 4 and the similar $^{EpCAM/GFP}$CAR T-cell numbers during the following observation period. Scale bars: 80 μm. E: Density of intravenously injected (CAR) T-cells (cells/mm$^3$) within the tumor on days 4, 6, 8, and 10 after receiving $^{EpCAM/GFP}$CAR T-cells (green; n = 5) or $^{GFP}$T-cells (gray; n = 5), as assessed by two-photon laser scanning microscopy. Mean ± SEM. *$p \leq 0.05$. F: Pooled tumor areas (mm$^2$) on days −1, 4, 6, 8, and 10 following intravenous injection of $^{EpCAM/GFP}$CAR T-cells (green; n = 6) or $^{GFP}$T-cells (gray; n = 6) determined by *in vivo* microscopy using epifluorescence. Mean ± SEM.

treated with $^{EpCAM/GFP}$CAR T-cells compared to controls receiving $^{GFP}$T-cells (3.6 ± 3 mm$^3$ *versus* 33.2 ± 6 mm$^3$), further confirming our results from *in vivo* microscopy (Figure 5a-k). Notably, there were no significant differences in the number of $^{EpCAM/GFP}$CAR T-cells within the remaining tumor tissue compared to $^{GFP}$T-cells in controls (Figure 5l). The distribution of fluorescent (CAR) T-cells across the tumor was comparable, and higher numbers were encountered within the tumor core

than in the border zone of the tumor (percentage of (CAR) T-cells within the tumor core in comparison to all intratumoral T-cells: $^{EpCAM/GFP}$CAR T-cells: 61.2 ± 8% *versus* $^{GFP}$T-cells: 69.0 ± 5) (Figure 5m). EpCAM expression was found in all tumors of both groups (**Supplementary Figure 2A-C**). Notably, tumors of mice which were treated with locally injected $^{EpCAM/GFP}$CAR T-cells showed strong EpCAM expression making it unlikely that antigen loss as an escape
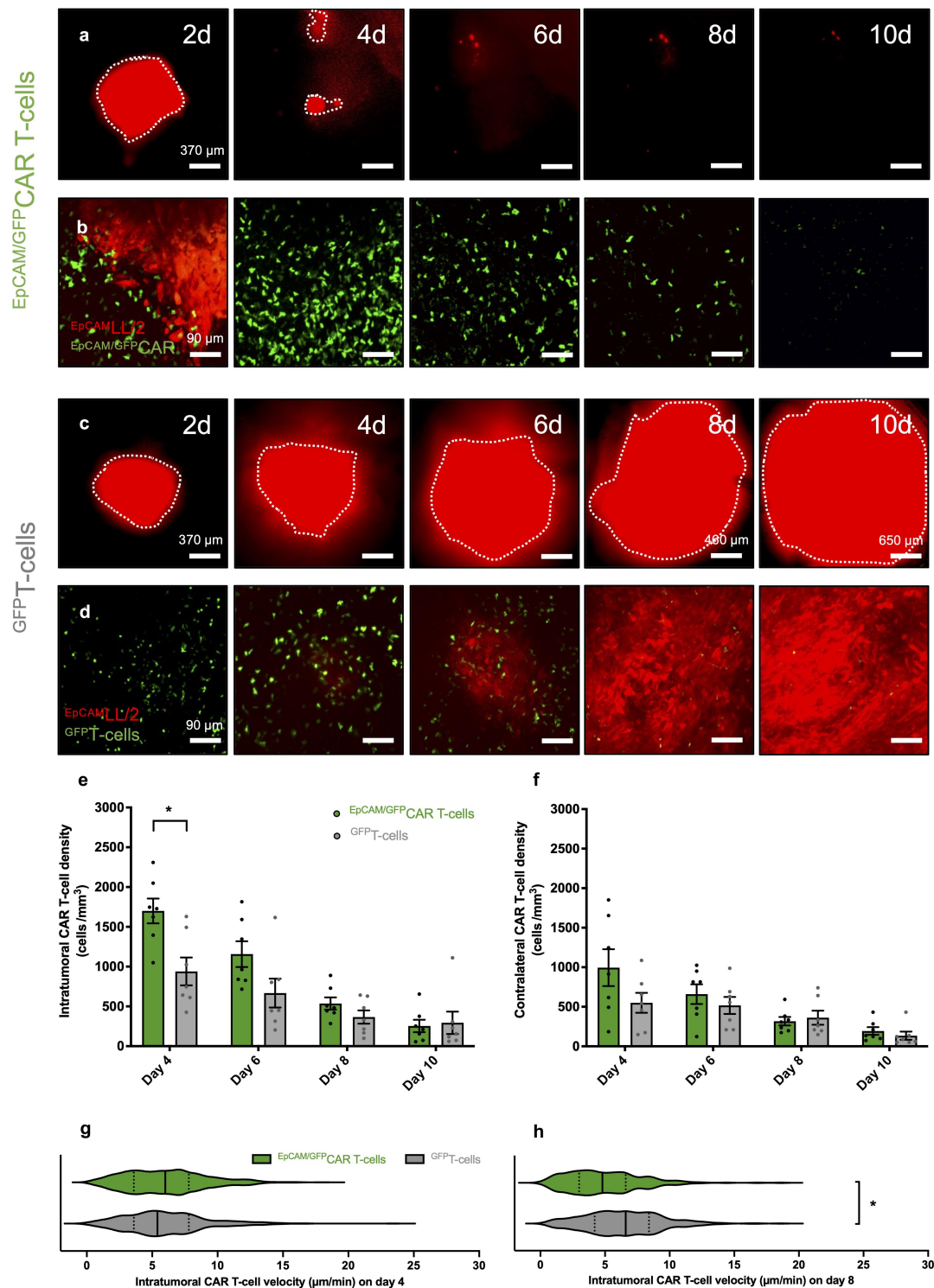
**Figure 3.** *In vivo* **CAR T-cell dynamics after intraparenchymal injection**. A-D: Representative *in vivo* images of brain tumors (red) on days 2, 4, 6, 8, and 10 after intraparenchymal injection of [EpCAM/GFP]CAR T-cells (green; A, B) or [GFP]T-cells (green; C, D) using epifluorescence (A, C; brain tumors delineated by dotted lines) and two-photon laser scanning microscopy (B, D; maximum intensity projections with 400 μm depth from the brain surface). Note the tumor regression and intratumoral CAR T-cell accumulation after local administration of [EpCAM/GFP]CAR T-cells. Scale bars: A, C: 370 μm (except [GFP]T-cells, day 8: 460 μm and day 10: 650 μm); B, D: 90 μm. E, F: Density of (CAR) T-cells (cells/mm$^3$) within the tumor (e) and the healthy contralateral brain hemisphere (f) on days 4, 6, 8, and 10 after locally receiving [EpCAM/GFP]CAR T-cells (green; n = 7) or [GFP]T-cells (gray; n = 7), as assessed by two-photon laser scanning microscopy. Mean ± SEM. G, H: Intratumoral (CAR) T-cell velocity (μm/min) determined by two-photon laser scanning microscopy on day 4 (g) and day 8 (h) after local injection of [EpCAM/GFP]CAR T-cells (green; n = 7) or [GFP]T-cells (gray; n = 7). Straight lines in the violin plot indicate the median, dotted lines indicate quartiles. *$p \leq 0.05$.

mechanism represents a relevant mechanism of therapy resistance in our model. Markers for tumor-associated macrophages and microglia (namely Iba1) or of M2-polarized macrophages (namely CD206) were strongly expressed in tumors of mice with were treated with locally injected [EpCAM/GFP]CAR T-cells or [GFP]T-cells (**Supplementary Figure 2D-G**).[22] Here, accumulation of CD206- and Iba1-positive cells was particularly observed in the tumor border zone.
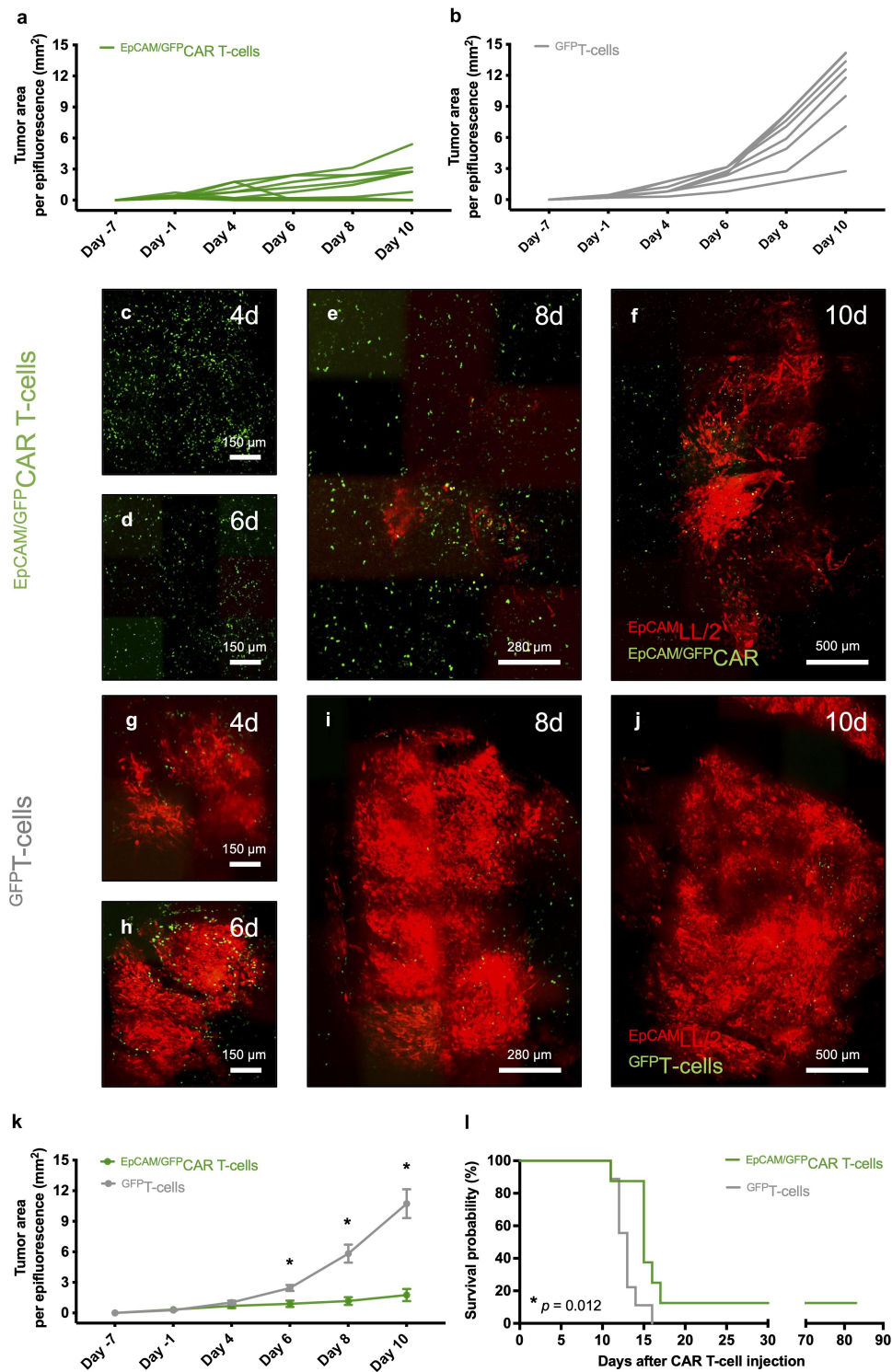
**Figure 4. Tumor growth and survival after intraparenchymal injection of CAR T-cells**. A, B: Individual tumor areas (mm²) measured by *in vivo* microscopy using epifluorescence on days −1, 4, 6, 8, and 10 after local injection of [EpCAM/GFP]CAR T-cells (A; n = 10) or [GFP]T-cells (B; n = 8). C-J: Brain tumor growth on days 4, 6, 8, and 10 after intraparenchymal injection of [EpCAM/GFP]CAR T-cells (c-f) or [GFP]T-cells (g-j) as illustrated by representative mosaics of multiple maximum intensity projections (with 400 μm depth from the brain surface) from two-photon laser scanning microscopy. [EpCAM/GFP]CAR T-cells or [GFP]T-cells are detected by their green fluorescent signal, and tumor cells are visualized based on their red fluorescent signal. Early in the observation period, [EpCAM/GFP]CAR T-cells were more evenly distributed throughout the tumor compared to [GFP]T-cells resulting in reduced tumor growth. Scale bars: C-D, G-H: 150 μm; E, I: 280 μm; F, J: 500 μm. K: Pooled tumor areas (mm²) on days −1, 4, 6, 8, and 10 following local injection of [EpCAM/GFP]CAR T-cells (green; n = 10) or [GFP]T-cells (gray; n = 8) determined by *in vivo* microscopy using epifluorescence. Mean ± SEM. *$p \leq 0.05$. L: Kaplan–Meier estimates of survival in mice with brain tumors (injected seven days prior to (CAR) T-cell injection) following treatment with [EpCAM/GFP]CAR T-cells (green; n = 8) or [GFP]T-cells (gray; n = 9).
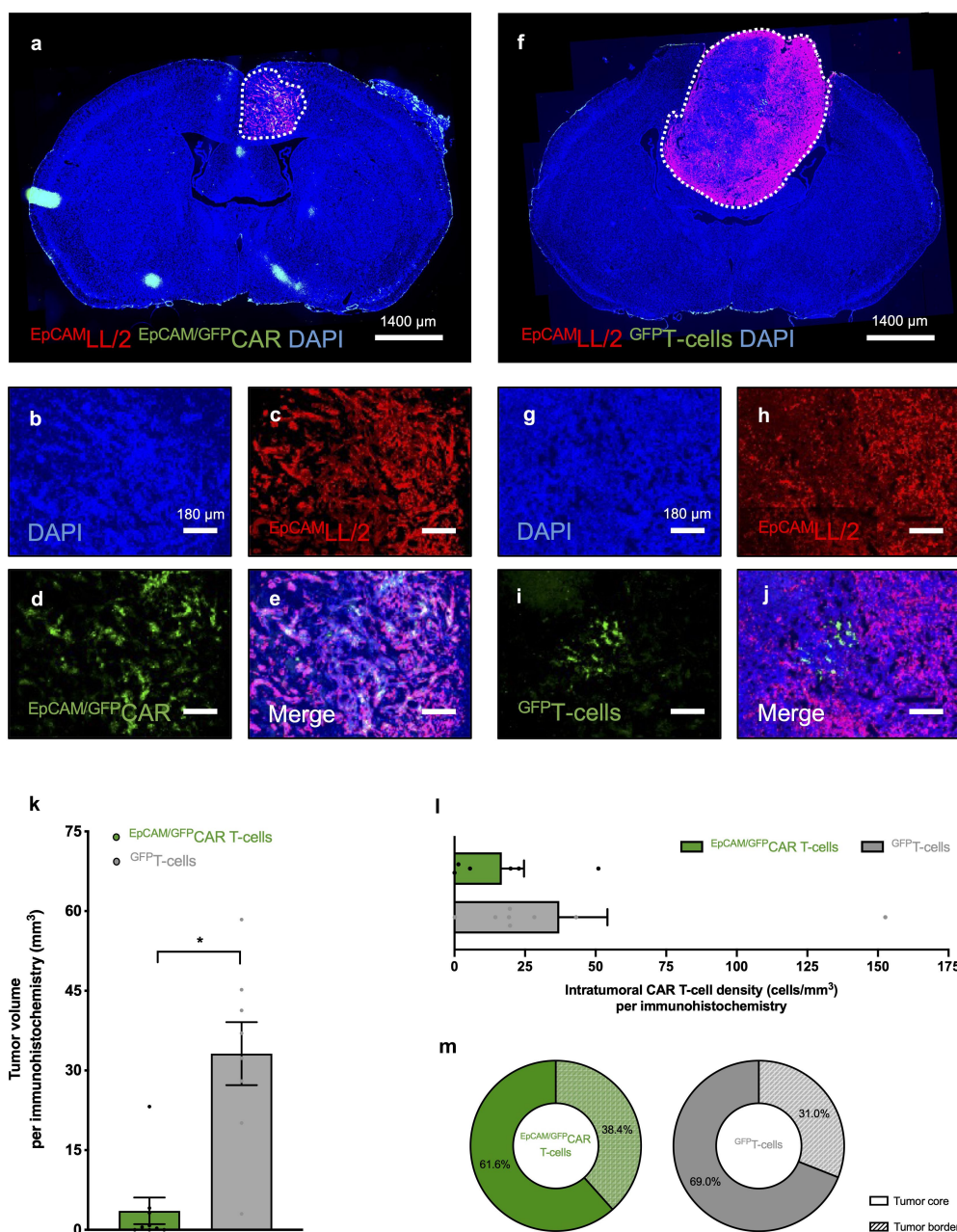
**Figure 5. Immunofluorescence characterization of tumor growth and intratumoral CAR T-cells following intraparenchymal CAR T-cell injection**. A-J: Histological sections of brains from mice with brain tumors excised 10 days after intraparenchymal injection of EpCAM/GFPCAR T-cells (a-e) or GFPT-cells (f-j). Sections were stained with an antibody against TdTomato to identify tumor cells (red), against GFP to visualize the (CAR) T-cell signal, and DAPI to allow detection of cell nuclei (blue). Tumors (dotted lines in A, F) were substantially smaller in mice which have received EpCAM/GFPCAR T-cells, whereas (CAR) T-cells were scattered through the tumor in scant numbers in both groups. B-E and G-J represent a selected intratumoral area from A and B, respectively. Scale bars: A, F: 1400 μm; B-E, G-J: 180 μm. K-M: Tumor volume (K; mm$^3$), intratumoral (CAR) T-cell density (L; cells/mm$^3$), and distribution of intratumoral (CAR) T-cells (M; percentage) on day 10 after injection of EpCAM/GFPCAR T-cells (green; n = 9) or GFPT-cells (gray; n = 8) determined by immunofluorescence. Mean ± SEM. *$p ≤ 0.05$.

## Discussion

The natural history of lung cancer patients with brain metastases is still devastating, and innovative therapeutic approaches are urgently needed for those patients.[1,3] We herein performed repetitive *in vivo* imaging through a cranial window to monitor lung cancer brain metastasis growth after intracranial CAR T-cell injection, which offered the exciting opportunity to assess real-time dynamics of CAR T-cells in the brain at a single-cell level. Based on this fully immunocompetent model, we were able to illustrate the promising anti-tumor activity of locally (but not systemically) injected EpCAM-directed CAR T-cells for brain metastases from lung cancer.

We found that treatment with CAR T-cells injected into the cerebral parenchyma resulted in significant decreased brain tumor growth and in selected cases led to complete tumor regression. These anti-tumor effects translated into a survival benefit of mice treated with CAR T-cells including long-lasting remission. It is noteworthy that we did not find any evidence of anti-tumorous effects after intravenous injection of CAR T-cells, which may highlight the potential of local application of immunotherapies. Similar findings have been made in

preclinical *in vivo* models assessing intracranially administered CAR T-cells for the treatment of primary CNS malignancies including CNS lymphoma,[21] medulloblastoma,[23] or glioblastoma,[24] as well as for secondary CNS malignancies such as breast cancer metastases.[25] Although the favorable results have encouraged (ongoing) clinical CAR T-cell trials for brain tumor patients,[6,7] to our knowledge none of these studies yet focus particularly on lung cancer patients with brain metastases. Our present study appears to support that CAR T-cell therapy might also warrant evaluation in individuals with brain metastases from lung cancer. Given that our preclinical findings were made in a fully immunocompetent murine model, our encouraging results may have substantial translational implications.

Our model allowed to dissect the *in vivo* dynamics of CAR T-cells, and our analysis at early days after local CAR T-cell injection showed a higher density of intratumoral CAR T-cells which compared to undirected T-cells serving as controls. This observation indicates enhanced proliferation, migration, and tumor infiltration of directed CAR T-cells. Although the exact mechanisms herein remain elusive, early antigen contact of the (EpCAM-directed) CAR T-cells with the (EpCAM-expressing) tumor cells might have contributed to these effects. Such an interaction substantially stimulates differentiation, proliferation, and survival of T-cells.[26,27] Accordingly, CAR T-cells in our model were characterized by lower velocities than undirected T-cells, which were previously described to reflect the interaction of cytotoxic T-cells with the targeted tumor cells.[20,21]

On a cautionary note, these CAR T-cell specific dynamics successively diminished during the observation period pointing toward insufficient persistence of CAR T-cell within the tumor tissue. Decreasing numbers of intratumoral CAR T cells were paralleled by tumor growth. Intratumoral CAR T-cell density as well as the distribution of the CAR T-cells within the tumor was comparable to controls for both systemically and locally injected CAR T-cells at the end of the *in vivo* experiments (as confirmed by *in vivo* microscopy as well as immunofluorescence). These findings seem consistent with preclinical and clinical reports of rapidly decreasing CAR T-cell numbers and T-cell exhaustion in other solid brain tumors such as gliomas.[28] Clinical trials for brain tumor patients evaluating concepts to counteract the insufficient persistence by stimulation of CAR T-cells with immunotherapies such as checkpoint inhibitors are ongoing (e.g. NCT04003649).[29] In this context, CAR T-cells entering the systemic circulating (and homing into lymph nodes) following intracranial injection have been identified as a reservoir protecting against local tumor recurrence in the CNS.[21,30] We were unable to detect any intravascular CAR T-cells in peripherally taken blood samples following local CAR T-cell injection, and it appears therefore unlikely that such a blood infiltration might have taken place in our study. If administered, the use of lymphodepletion prior to CAR T-cell administration could have increased the systemic quantity and persistence of CAR T-cells, which might have also enhanced the effects of systemically injected CAR T-cells by boosting their insufficient intravascular expansion.[31] Also, optimization of the provided CAR T-cell dosage may further boost the therapeutic anti-tumor success of such therapy.

However, the fact that locally injected CAR T-cells did not migrate into the systemic circulation may also be beneficial in reducing CAR T-cell-mediated side effects. Such toxicities most frequently include neurologic symptoms such as seizures,[32,33] a sepsis-like phenotype entitled 'cytokine release syndrome,'[33,34] hematological effects,[35] and even fatalities have been reported.[36] Given the expression of EpCAM as a pan-epithelial cell marker on healthy alveolar tissue,[37] on-target /off-tumor effects due to shared expression of target antigens on neoplastic and healthy tissue might be particularly problematic in EpCAM-directed CAR T-cells.[38] Importantly, we did not encounter any evidence for clinically relevant side effects in our fully immunocompetent model, even though the scFv used in our CAR construct (G8.8) has been shown to recognize murine EpCAM present in most murine epithelial tissues. However, these results cannot thoroughly predict on-target /off-tumor side effects in humans due to the translational nature of our study or the relatively small sample size; and we also did not observe such effects after systemic CAR T-cell injection. The clinically relevant safety profile of EpCAM-directed CAR T-cells is currently being evaluated in prospective cohorts (e.g. in an ongoing phase I/II trial on EpCAM-directed CAR T-cells for non-CNS cancer, NCT04151186).

Most importantly, we made use of CAR T-cells injected into the cerebral parenchyma adjacent to the brain tumor. Whereas we and others observed promising anti-tumor effects using this approach,[30,39] systemic routes of administration (including intravenous or intraperitoneal injection) have shown less encouraging results in CNS disease.[21,30,40] Accordingly, we did not detect efficient anti-tumor effects after systemic administration of CAR T-cells. It remains to be noted that brain metastases are often disseminated within the cerebral parenchyma, and systemic routes might theoretically be particularly beneficial in controlling or preventing micrometastatic disease. Based on our model, the number of intratumoral [GFP]T-cells in the control group quantified per immunofluorescence might not only be a result of T-cell migration into the tumor but might also be due to the more extensive tumor growth toward the injection site of [GFP]T-cells compared to the treatment group. This could potentially have resulted in a quantification which not only reflects T-cell migration but also tumor overgrowth and might therefore have contributed to an overestimation of the infiltration capacities of undirected T-cells. Brain metastases from lung cancer are particularly prone to creating an immunosuppressive niche composed of neoplastic as well as non-neoplastic cells including tumor-associated macrophages and microglia, as demonstrated by strong expression of Iba1 as well as the M2-marker CD206 in the tumor border zone.[12] It remains to be seen whether the immunosuppressive microenvironment of brain metastases from lung cancer may represent an interesting target to further increase the efficiency of CAR T-cell-based immunotherapy.[15,41]

The *in vivo* dynamics and anti-tumor effects of CAR T-cells were followed in the cranial window model using two-photon laser scanning microscopy. Contrary to conventional histological approaches, this allowed for repetitive longitudinal analysis of CAR T-cells over weeks in each individual mouse. On a cautionary note, one mouse in which we failed to detect any tumor following local CAR T-cell injection via *in vivo*

microscopy had some residual tumor growth below visualizable depths when brains were assessed via immunofluorescence, which illustrates the importance of complementing findings based on *in vivo* imaging with other methods. Moreover, intraparenchymal tumor cell injection provided reliable tumor take but does not necessarily mimic metastatic growth by hematological dissemination of individual tumor cells. Despite *in vivo* models to reproduce the individual steps of brain metastasis formation are available based upon intra-arterial tumor cell injections,[12] such approaches result in metastases of variable size and localization. Only the herein used intraparenchymal tumor cell injection allowed to standardize the distance between the brain tumor and the CAR T-cell injection. Although we found excellent imaging quality and reliable orthotopic tumor growth, we cannot exclude sterile neuroinflammation and microglial activation due to window preparation and injection of tumor cells or CAR T-cells as previously described.[12] Notably, inflammatory reactions would theoretically be present in both groups, which indicate that such a reaction alone is not sufficient to induce tumor regression or trafficking of CAR T-cells into the tumor.

Collectively, the present study highlights the encouraging anti-tumor effects of intracranially (but not systemically) injected CAR T-cells against solid brain metastases from lung cancer. CAR T-cell migration towards the tumor as well as intratumoral CAR T-cell accumulation were associated with tumor regression early after the intraparenchymal injection; however, decreasing CAR T-cell numbers during the late observation period suggest insufficient persistence, which might be paralleled by tumor regrowth. Given the complex interaction of CAR T-cells with the immunosuppressive tumor microenvironment of brain metastases, improved CAR design and the choice of concurrent therapies may further boost the success of CAR T-cell therapy for brain metastases. The herein introduced fully immunocompetent murine model might be a useful tool to evaluate such approaches.

## Availability of data and materials

Coded data can be accessed upon qualified request from the authors.

## Ethics approval and consent to participate, consent for publication

We take full responsibility for this original research. We also would like to confirm that this paper has not been submitted to another journal and has not been published in whole or in part elsewhere previously. I have full access to all data, and I have the right to publish any and all data. Clinical metadata was collected with IRB approval and informed consent. All authors have read and agreed to the submission of this study to *Onco-Immunology* and to the conditions noted on the Authorship Agreement Form.

## Disclosure statement

Tao Xu, No disclosures; Philipp Karschnia, No disclosures; Bruno L. Cadilha, No disclosures; Sertac Dede, No disclosures; Michael Lorenz, No disclosures; Niklas Seewaldt, No disclosures; Elene Nikolaishvili, No disclosures; Katharina Müller, No disclosures; Jens Blobner, No disclosures; Nico Teske, No disclosures; Julika J. Herold, No disclosures; Kai Rejeski, Kite/Gilead: Research funding and travel support, Novartis:

Honoraria, BMS/CELGENE: Consultancy, Honoraria; Sigrid Langer, No disclosures; Hannah Obeck, No disclosures; Theo Lorenzini, No disclosures; Matthias Mulazzani, No disclosures; Wenlong Zhang, No disclosures; Hellen Ishikawa-Ankerhold, No disclosures; Veit R. Buchholz, No disclosures; Marion Subklewe, No disclosures; Niklas Thon, No disclosures; Andreas Straube, No disclosures; Joerg-Christian Tonn, Research grants from Novocure and Munich Surgical Imaging, and Royalties from Springer Publisher Intl; Sebastian Kobold, S.K. has received honoraria from TCR2 Inc, Novartis, BMS and GSK, S.K. is an inventor of several patents in the field of immuno-oncology, S.K. received license fees from TCR2 Inc and Carina Biotech, S.K. received research support from TCR2 Inc. and Arcus Bioscience for work unrelated to the manuscript. Louisa von Baumgarten, No disclosures.

## References

1. Achrol AS, Rennert RC, Anders C, Soffietti R, Ahluwalia MS, Nayak L, Peters S, Arvold ND, Harsh GR, Steeg PS, et al. Brain metastases. Nat Rev Dis Primers. 2019;5(1):5. doi:10.1038/s41572-018-0055-y.
2. Shaw AT, Bauer TM, de Marinis F, Felip E, Goto Y, Liu G, Mazieres J, Kim D-W, Mok T, Polli A, et al. First-Line Lorlatinib or Crizotinib in Advanced ALK -Positive Lung Cancer. N Engl J Med. 2020;383(21):2018–2029. doi:10.1056/NEJMoa2027187.
3. Karschnia P, Le Rhun E, Vogelbaum MA, et al. The evolving role of neurosurgery for central nervous system metastases in the era of personalized cancer therapy. Eur J Cancer. 2021;156:93–108. doi:10.1016/j.ejca.2021.07.032.
4. Goldberg SB, Schalper KA, Gettinger SN, Mahajan A, Herbst RS, Chiang AC, Lilenbaum R, Wilson FH, Omay SB, Yu JB, et al. Pembrolizumab for management of patients with NSCLC and brain metastases: long-term results and biomarker analysis from

a non-randomised, open-label, phase 2 trial. Lancet Oncol. 2020;21 (5):655–663. doi:10.1016/S1470-2045(20)30111-X.

5. Chong EA, Ruella M, Schuster SJ. Five-Year Outcomes for Refractory B-Cell Lymphomas with CAR T-Cell Therapy. N Engl J Med. 2021;384(7):673–674. doi:10.1056/NEJMc2030164.

6. Karschnia P, Teske N, Thon N, Subklewe M, Tonn J-C, Dietrich J, von Baumgarten L. CAR T-Cells for Glioblastoma Current Concepts, Challenges and Future Perspectives. Neurology. 2021;97(5):218–230. doi:10.1212/WNL.0000000000012193.

7. Karschnia P, Blobner J, Teske N, et al. CAR T-Cells for CNS Lymphoma: driving into New Terrain? Cancers. 2021;14(1):13. doi:10.3390/cancers14010013.

8. Sebastian M, Passlick B, Friccius-Quecke H, Jäger M, Lindhofer H, Kanniess F, Wiewrodt R, Thiel E, Buhl R, Schmittel A, et al. Treatment of non-small cell lung cancer patients with the trifunctional monoclonal antibody catumaxomab (anti-EpCAM x anti-CD3): a phase I study. Cancer Immunol Immunother. 2007;56(10):1637–1644. doi:10.1007/s00262-007-0310-7.

9. Kim Y, Kim HS, Cui ZY, Lee H-S, Ahn JS, Park CK, Park K, Ahn M-J. Clinicopathological implications of EpCAM expression in adenocarcinoma of the lung. Anticancer Res. 2009;29:1817–1822.

10. Spizzo G, Fong D, Wurm M, Ensinger C, Obrist P, Hofer C, Mazzoleni G, Gastl G, Went P. EpCAM expression in primary tumour tissues and metastases: an immunohistochemical analysis. J Clin Pathol. 2011;64(5):415–420. doi:10.1136/jcp.2011.090274.

11. Li W, Zhou Y, Wu Z, Shi Y, Tian E, Zhu Y, Wang T, Dou W, Meng X, Chen M, et al. Targeting wnt signaling in the tumor immune microenvironment to enhancing EpCAM CAR T-Cell therapy. Front Pharmacol. 2021;12:724306. doi:10.3389/fphar.2021.724306.

12. Zhang W, Karschnia P, von Mücke-Heim IA, Mulazzani M, Zhou X, Blobner J, Mueller N, Teske N, Dede S, Xu T, et al. In vivo two-photon characterization of tumor-associated macrophages and microglia (TAM/M) and CX3CR1 during different steps of brain metastasis formation from lung cancer. Neoplasia. 2021;23(11):1089–1100. doi:10.1016/j.neo.2021.09.001.

13. Karches CH, Benmebarek MR, Schmidbauer ML, Kurzay M, Klaus R, Geiger M, Rataj F, Cadilha BL, Lesch S, Heise C, et al. Bispecific antibodies enable synthetic agonistic receptor-transduced T cells for tumor immunotherapy. Clin Cancer Res. 2019;25(19):5890–5900. doi:10.1158/1078-0432.CCR-18-3927.

14. Lesch S, Blumenberg V, Stoiber S, Gottschlich A, Ogonek J, Cadilha BL, Dantes Z, Rataj F, Dorman K, Lutz J, et al. T cells armed with C-X-C chemokine receptor type 6 enhance adoptive cell therapy for pancreatic tumours. Nat Biomed Eng. 2021;5 (11):1246–1260. doi:10.1038/s41551-021-00737-6.

15. Cadilha BL, Benmebarek MR, Dorman K, Oner A, Lorenzini T, Obeck H, Vänttinen M, Di Pilato M, Pruessmann JN, Stoiber S, et al. Combined tumor-directed recruitment and protection from immune suppression enable CAR T cell efficacy in solid tumors. Sci Adv. 2021;7(24). doi:10.1126/sciadv.abi5781.

16. Rapp M, Grassmann S, Chaloupka M, Layritz P, Kruger S, Ormanns S, Rataj F, Janssen K-P, Endres S, Anz D, et al. C-C chemokine receptor type-4 transduction of T cells enhances interaction with dendritic cells, tumor infiltration and therapeutic efficacy of adoptive T cell transfer. Oncoimmunology. 2016;5(3): e1105428. doi:10.1080/2162402X.2015.1105428.

17. Winkler F, Kienast Y, Fuhrmann M, Von Baumgarten L, Burgold S, Mitteregger G, Kretzschmar H, Herms J. Imaging glioma cell invasion in vivo reveals mechanisms of dissemination and peritumoral angiogenesis. Glia. 2009;57(12):1306–1315. doi:10.1002/glia.20850.

18. Kienast Y, von Baumgarten L, Fuhrmann M, Klinkert WEF, Goldbrunner R, Herms J, Winkler F. Real-time imaging reveals the single steps of brain metastasis formation. Nat Med. 2010;16 (1):116–122. doi:10.1038/nm.2072.

19. Bakker R, Tiesinga P, Kötter R. The scalable brain atlas: instant web-based access to public brain atlases and related content. Neuroinformatics. 2015;13(3):353–366. doi:10.1007/s12021-014-9258-x.

20. Boissonnas A, Fetler L, Zeelenberg IS, Hugues S, Amigorena S. In vivo imaging of cytotoxic T cell infiltration and elimination of a solid tumor. J Exp Med. 2007;204(2):345–356. doi:10.1084/jem.20061890.

21. Mulazzani M, Fräßle SP, von Mücke-Heim I, Langer S, Zhou X, Ishikawa-Ankerhold H, Leube J, Zhang W, Dötsch S, Svec M, et al. Long-term in vivo microscopy of CAR T cell dynamics during eradication of CNS lymphoma in mice. Proc Natl Acad Sci U S A. 2019;116(48):24275–24284. doi:10.1073/pnas.1903854116.

22. Mantovani A, Allavena P, Marchesi F, Garlanda C. Macrophages as tools and targets in cancer therapy. Nat Rev Drug Discov. 2022;21 (11):799–820. doi:10.1038/s41573-022-00520-5.

23. Donovan LK, Delaidelli A, Joseph SK, Bielamowicz K, Fousek K, Holgado BL, Manno A, Srikanthan D, Gad AZ, Van Ommeren R, et al. Locoregional delivery of CAR T cells to the cerebrospinal fluid for treatment of metastatic medulloblastoma and ependymoma. Nat Med. 2020;26(5):720–731. doi:10.1038/s41591-020-0827-2.

24. Wang D, Starr R, Chang WC, et al. Chlorotoxin-directed CAR T cells for specific and effective targeting of glioblastoma. Sci Transl Med. 2020;2020:12.

25. Priceman SJ, Tilakawardane D, Jeang B, et al. Regional delivery of chimeric antigen receptor-engineered t cells effectively targets HER2(+) breast cancer metastasis to the brain. Clin Cancer Res. 2018;24(1):95–105. doi:10.1158/1078-0432.CCR-17-2041.

26. Kaech SM, Ahmed R. Memory CD8+ T cell differentiation: initial antigen encounter triggers a developmental program in naïve cells. Nat Immunol. 2001;2(5):415–422. doi:10.1038/87720.

27. Shyer JA, Flavell RA, Bailis W. Metabolic signaling in T cells. Cell Res. 2020;30(8):649–659. doi:10.1038/s41422-020-0379-5.

28. Brown CE, Badie B, Barish ME, Weng L, Ostberg JR, Chang W-C, Naranjo A, Starr R, Wagner J, Wright C, et al. Bioactivity and safety of IL13Rα2-Redirected chimeric antigen receptor CD8+ T cells in patients with recurrent glioblastoma. Clin Cancer Res. 2015;21 (18):4062–4072. doi:10.1158/1078-0432.CCR-15-0428.

29. Blaeschke F, Stenger D, Apfelbeck A, Cadilha BL, Benmebarek M-R, Mahdawi J, Ortner E, Lepenies M, Habjan N, Rataj F, et al. Augmenting anti-CD19 and anti-CD22 CAR T-cell function using PD-1-CD28 checkpoint fusion proteins. Blood Cancer J. 2021;11(6):108. doi:10.1038/s41408-021-00499-z.

30. Wang X, Huynh C, Urak R, Weng L, Walter M, Lim L, Vyas V, Chang W-C, Aguilar B, Brito A, et al. The cerebroventricular environment modifies CAR T cells for potent activity against both central nervous system and systemic lymphoma. Cancer Immunol Res. 2021;9(1):75–88. doi:10.1158/2326-6066.CIR-20-0236.

31. Sampson JH, Choi BD, Sanchez-Perez L, Suryadevara CM, Snyder DJ, Flores CT, Schmittling RJ, Nair SK, Reap EA, Norberg PK, et al. EGFRvIII mCAR-modified T-cell therapy cures mice with established intracerebral glioma and generates host immunity against tumor-antigen loss. Clin Cancer Res. 2014;20(4):972–984. doi:10.1158/1078-0432.CCR-13-0709.

32. Sokolov E, Karschnia P, Benjamin R, Hadden RDM, Elwes RCD, Drummond L, Amin D, Paiva V, Pennisi A, Herlopian A, et al. Language dysfunction-associated EEG findings in patients with CAR-T related neurotoxicity. BMJ Neurology Open. 2020;2(1): e000054. doi:10.1136/bmjno-2020-000054.

33. Karschnia P, Jordan JT, Forst DA, Arrillaga-Romany IC, Batchelor TT, Baehring JM, Clement NF, Gonzalez Castro LN, Herlopian A, Maus MV, et al. Clinical presentation, management, and biomarkers of neurotoxicity after adoptive immunotherapy with CAR T cells. Blood. 2019;133(20):2212–2221. doi:10.1182/blood-2018-12-893396.

34. Fajgenbaum DC, June CH, Longo DL. Cytokine Storm. N Engl J Med. 2020;383(23):2255–2273. doi:10.1056/NEJMra2026131.

35. Rejeski K, Perez Perez A, Sesques P, Hoster E, Berger C, Jentzsch L, Mougiakakos D, Frölich L, Ackermann J, Bücklein V, et al. CAR-HEMATOTOX: a model for CAR T-cell related hematological toxicity in relapsed/refractory large B-cell lymphoma. Blood. 2021;138(24):2499–2513. doi:10.1182/blood.2020010543.

36. Karschnia P, Strübing F, Teske N, Blumenberg V, Bücklein VL, Schmidt C, Schöberl F, Dimitriadis K, Forbrig R, Stemmler H-J, et al. Clinicopathologic findings in fatal neurotoxicity after adoptive immunotherapy with CD19-Directed CAR T-Cells. HemaSphere. 2021;5(3):e533. doi:10.1097/HS9.0000000000000533.

37. Hasegawa K, Sato A, Tanimura K, Uemasu K, Hamakawa Y, Fuseya Y, Sato S, Muro S, Hirai T. Fraction of MHCII and EpCAM expression characterizes distal lung epithelial cells for alveolar type 2 cell isolation. Respir Res. 2017;18(1):150. doi:10.1186/s12931-017-0635-5.

38. Qin D, Li D, Zhang B, Chen Y, Liao X, Li X, Alexander PB, Wang Y, Li Q-J. Potential lung attack and lethality generated by EpCAM-specific CAR-T cells in immunocompetent mouse models. Oncoimmunology. 2020;9(1):1806009. doi:10.1080/2162402X.2020.1806009.

39. Brown CE, Alizadeh D, Starr R, Weng L, Wagner JR, Naranjo A, Ostberg JR, Blanchard MS, Kilpatrick J, Simpson J, et al. Regression of glioblastoma after chimeric antigen receptor T-Cell therapy. N Engl J Med. 2016;375(26):2561–2569. doi:10.1056/NEJMoa1610497.

40. Agliardi G, Liuzzi AR, Hotblack A, De Feo D, Núñez N, Stowe CL, Friebel E, Nannini F, Rindlisbacher L, Roberts TA, et al. Intratumoral IL-12 delivery empowers CAR-T cell immunotherapy in a pre-clinical model of glioblastoma. Nat Commun. 2021;12(1):444. doi:10.1038/s41467-020-20599-x.

41. Karschnia P, Xu T, Fitzinger E, Saliger JC, Blobner J, Teske N, von Muecke-Heim I-A, Langer S, Konhäuser M, Ishikawa-Ankerhold H, et al. TAMI-02. Depletion Of Intratumoral Tumor-Associated Macrophages And Microglia (Tam/M) Improves Checkpoint-Inhibition Therapy For Brain Metastasis From Lung Cancer. Neuro-Oncology. 2021;23(Supplement_6):vi198–vi198. doi:10.1093/neuonc/noab196.786.